Effects of nodal planes on strong-field ionization and high-order-harmonic generation in ring-type molecules

A. F. Alharbi,[1,2] A. E. Boguslavskiy,[1] N. Thiré,[3] G. S. Thekkadath,[4] S. Patchkovskii,[4] B. E. Schmidt,[3] F. Légaré,[3] T. Brabec,[1] V. R. Bhardwaj,[1,*] and M. Spanner[4,†]

[1]*Department of Physics, University of Ottawa, 150 Louis-Pasteur, Ottawa, Ontario K1N 6N5, Canada*
[2]*King Abdulaziz City for Science and Technology (KACST), P.O. Box 6086, Riyadh 11442, Saudi Arabia*
[3]*INRS-EMT, Advanced Laser Light Source, 1650 Lionel-Boulet Bvd, Varennes, Quebec, J3X1S2, Canada*
[4]*National Research Council Canada, 100 Sussex Drive, Ottawa, Ontario, K1A 0R6 Canada*

(Received 9 January 2016; published 3 October 2017)

We measure the ellipticity dependence of high-harmonic generation (HHG) from unaligned gas-phase ensembles of the five-membered ring molecules 2,3-dihydrofuran (C_4H_6O), furan (C_4H_4O), and thiophene (C_4H_4S). As is normally the case, the HHG emission is suppressed for increased ellipticity since the recollision wave packet leading to HHG is steered away from the parent ion for large ellipticity. However, through comparison with computations of the first step in HHG, namely, strong-field ionization (SFI), we show that the observed differences in the ellipticity dependence for the three molecular species reflect the lateral momentum distributions of the continuum electron responsible for HHG, which in turn provides information about the particular orientation between the molecular axis and the laser field that maximizes the SFI probability. Strikingly, and contrary to the conventional wisdom in the strong-field community, we find that for furan and thiophene the most probable orientation for SFI occurs when the electric field of the laser is aligned near a nodal plane of the corresponding ionizing orbital. 2,3-dihydrofuran, on the other hand, follows the standard expectation that the most probable orientation for SFI occurs when the electric field is aligned away from any nodal plane.

DOI: 10.1103/PhysRevA.96.043402

Strong-field ionization (SFI) is a fundamental process that occurs during the interaction of intense laser fields with atoms and molecules [1–4]. It lies at the core of high-harmonic generation (HHG), a process where the laser first ionizes a molecule through SFI followed by laser-driven acceleration of the continuum electron, which then recollides and recombines with the parent ion through the emission of a burst of XUV radiation [5,6]. The understanding and development of HHG has lead to the rise of attosecond science [7] and novel methods to probe molecular structure and dynamics, for example, molecular orbital tomography [8–10] and high-harmonic spectroscopy [11–14]. The occupied orbitals in the multielectronic wave functions of molecules often possess rich nodal structures. These nodal structures can modulate the SFI rate [15,16] as well as add non-atomic-like phase [17] and amplitude [18–21] modulations to the continuum electron wave packets when the electric field of the ionizing laser is aligned along certain directions relative to the molecular axis. Of particular relevance to our paper, the conventional wisdom in the strong-field community maintains that ionization should be suppressed when the electric field of the laser points along, or near, nodal planes of the orbitals. This expectation was first derived using the strong-field approximation for diatomics by Muth-Böhm *et al.* [15] and has been experimentally confirmed for various small molecules [22–24]. However, as larger molecules are being explored, this expectation may no longer apply [25].

In this letter, we investigate the effects of orbital nodal planes on the strong-field response of the ring-type molecules furan (C_4H_4O), 2,3-dihydrofuran (C_4H_6O), and thiophene (C_4H_4S). We measured HHG signals driven by elliptically polarized pulses for randomly oriented gas-phase samples for each molecular species. When elliptically polarized pulses are used to drive HHG, the continuum electron launched through SFI is deflected away from the parent ion, and hence increasing the ellipticity leads to a decrease in the recombination rate and the HHG signal [26,27]. Since this decay depends on the lateral momentum spread of the continuum wave packet, which, for example, is Gaussian for atomic systems, [28–30], its fingerprints can be obtained from the dependence of the intensity of harmonics on laser ellipticity. We measure that the HHG signals from the different molecular species show different dependences on the ellipticity, implying that the continuum wave packets for each molecule have different lateral momentum distributions.

Using the TD-RIS method [31,32], we compute the structure of the continuum electron wave packets following SFI, and demonstrate qualitative agreement between the computed lateral momentum widths of the continuum wave packets and the ellipticity dependence of HHG. Computational results also demonstrate that two of the molecular species (furan and thiophene) ionize with highest probability when the electric field of the laser is oriented along directions that lie close to the nodal planes, in sharp contrast with the standard SFI response of diatomics and triatomics. In such cases, the liberated electron wave packet carries the orbital nodes into the continuum, thereby increasing the lateral momentum of the continuum wave packet, which leads to the observed differences in the ellipticity dependence of HHG for the studied molecular species.

The experiment was conducted at Advanced Laser Light Source (ALLS) facility in Varennes, Canada. The light source

*ravi.bhardwaj@uottawa.ca
†michael.spanner@nrc.ca

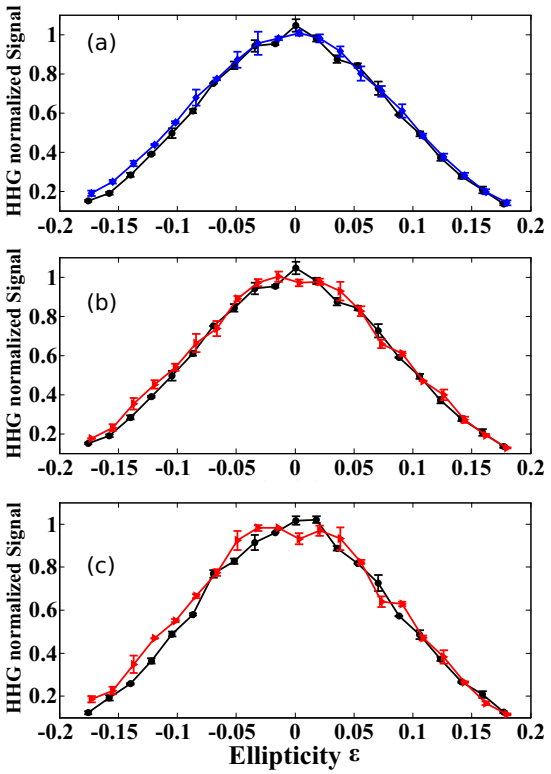

FIG. 1. The ellipticity dependence of the 41st harmonic for 2,3-dihydrofuran (black circles) vs (a) furan (blue squares) and (b) thiophene (red triangles). (c) Similar to (b) but for the 45th harmonic. at a laser intensity of 3×10^{13} W/cm^2 and a wavelength of 1800 nm.

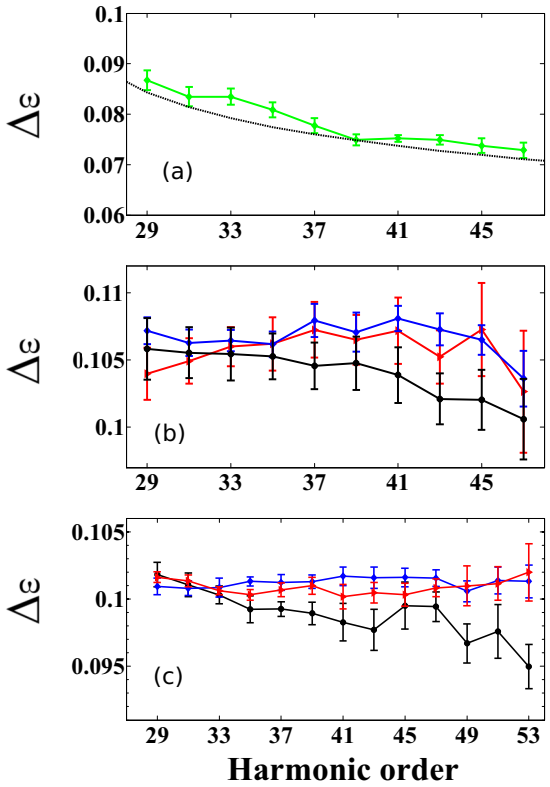

FIG. 2. (a) The ellipticity width $\Delta\epsilon$ as a function of harmonic order for Argon (green diamonds) at a laser intensity of 8×10^{13} W/cm^2. The dashed curve show the calculated widths. (b, c) The ellipticity width $\Delta\epsilon$ as a function of harmonic order for 2,3-dihydrofuran (black circles), thiophene (red triangles) and furan (blue squares) at two different laser intensities 3×10^{13} W/cm^2 (b) and 4×10^{13} W/cm^2 (c). The experiments were done with a laser wavelength of 1800 nm. The errors bars represent the 95% of the confidence interval of the Gaussian fits.

is described in details in Ref. [33]. Harmonic emission was generated by focusing mid infrared (1800 nm, 50 fs) pulses with a 50 cm CaF_2 lens into a 100 Hz pulsed gas jet. The ellipticity of the incident light was controlled by a combination of an adjustable half-wave plate and a fixed quarter-wave plate. This arrangement ensured that the main axis of the ellipse is fixed in space. The harmonic generation process was optimized to favor short trajectory harmonics and suppress the long trajectories. The emitted harmonics were recorded by a detection system composed of a grating, a microchannel plate (MCP) coupled to a phosphor screen and a charge-coupled device (CCD) camera. The vapor pressure of the molecular liquids was used to introduce them into the pulsed valve without heating or utilizing a carrier gas. The molecular gas inside the interaction volume was randomly oriented with a density on the order of 10^{17} cm^{-3}. All chemicals were obtained from Sigma-Aldrich with purities of 99%.

For the current study, we selected three organic molecules sharing the same ring size: 2,3-dihydrofuran, furan, and thiophene. In contrast to the first molecule, furan and thiophene are aromatic molecules whose two highest occupied molecular orbitals are fully delocalized π orbitals.

Figure 1(a) show the yields of the 41st harmonic as a function of laser ellipticity ϵ, defined as the ratio between the minor and major components of the driving laser field, for 2,3-dihydrofuran compared to furan. Similarly, we compare the dependence of the 41st and 45th harmonics in 2,3-dihrofuran and thiophene in Figs. 1(b) and 1(c) respectively.

Two interesting features can be observed. First, the response of the high harmonic yield to the ellipticity variation is weaker for both furan and thiophene as compared to 2,3-dihydrofuran. This suggests that the lateral momentum spread of the recollision wave packet is larger in furan and thiophene as compared to 2,3-dihydrofuran. Second, the dependence is slightly flatter around linear polarization in higher order harmonics in thiophene.

To gain more insight into the dissimilarities between the molecules, we consider how the ellipticity dependence changes with harmonic order. The experimental data were fitted with a Gaussian profile to extract the ellipticity width $\Delta\epsilon$ defined as the ellipticity value at which the harmonic yield drops to 50% compared to the value at linear polarization. Figure 2(a) shows $\Delta\epsilon$ as a function of harmonic order at 1800 nm for the three molecular systems and Ar for comparison. For Ar, $\Delta\epsilon$ decreases with increasing harmonic order, consistent with the fact that, for short trajectories, the travel time of the electron in the continuum is greater for higher harmonic orders leading to a larger relative displacement at recombination. The solid line shows the calculated $\Delta\epsilon$ using the semiclassical approach [34] and assuming a Gaussian shape for the continuum electron wave packet [28–30]. The

calculated values are in good agreement with the experimental data.

The lateral momentum scales inversely with the ionization potential of atoms. In molecules, since the ionization potential is much lower than that of Ar, for a given intensity $\Delta\epsilon$ can be expected to be larger compared to Ar. Furthermore, the higher angular momentum components generally present in molecular orbitals leads to an addition increase in $\Delta\epsilon$ for molecular systems [18]. Figures 2(b) and 2(c) show $\Delta\epsilon$ as a function of harmonic order for the three molecules at a laser intensity of 3×10^{13} W/cm^2 (4×10^{13} W/cm^2). The second set has a better statistical behavior because of the higher harmonic flux. In general, $\Delta\epsilon$ is a decreasing function of harmonic order in 2,3-dihydrofuran, similar to that of Ar. In contrast, the ellipticity widths in furan and thiophene does not decrease with the harmonic order and, generally, have larger values suggesting that the lateral momentum spread in these two molecular systems share similar qualitative characteristics that are different from those of 2,3-dihydrofuran.

In order to understand the experimental differences in the ellipticity dependence, we carry out time-dependent Schrödinger equation calculations of the ionization process using the time-dependent resolution-in-ionic-state (TD-RIS) method [31,32]. The computational details of both the electronic structure and the ionization computations appear in Ref. [35]. In addition to the details specified in that paper, here we make use of an effective core potential [36] for the S atom in thiophene. We calculate the SFI probabilities using a single half-cycle of the 1800 nm laser field, which allows us to focus on the subcycle ionization probabilities that are relevant to HHG. Further, the use of a half-cycle pulse is also important to retain the directionality of the subcycle orientation-dependent SFI probability: running the computation for a full cycle and/or a multicycle pulse would necessarily lose the directional SFI information since it would include ionization for a given electric field direction as well as the opposite direction when the field changes sign on the following half-cycle.

In Ref. [35] it was calculated that only ionization to the ground state of the cation (D_0 channel) is important for 2,3-dihydrofuran, while for furan and thiophene both the D_0 and the D_1 channels contribute. The orientation-dependent SFI probabilities for these active channels are shown in Fig. 3. For 2,3-dihydrofuran, there are two lobes of strong ionization. The fact that these two lobes show slightly different peak ionization yields reflects the fact that 2,3-dihydrofuran has broken symmetry (it has C1 symmetry). These two lobes appear at angles that do not lie along nodal planes.

For furan and thiophene, the D_0 channel shows two broad lobes of high SFI probability centered along the plane of the molecule with the peak angle of SFI is located at approximately 30° away from the the molecular plane. However, there is very high probability (only about 10% lower than at 30°) for ionization directly along a plane that coincides with a nodal plane of the corresponding Dyson orbital for these two D_0 channels; there is no strong suppression of the SFI rate along these nodal planes. The D_1 channel in furan has peaks of the ionization yield pointing away from the nodal planes, while the D_1 channel in thiophene has three peaks in the ionization yield with two pointing away from the nodal plane and the third pointing directly along a nodal plane.

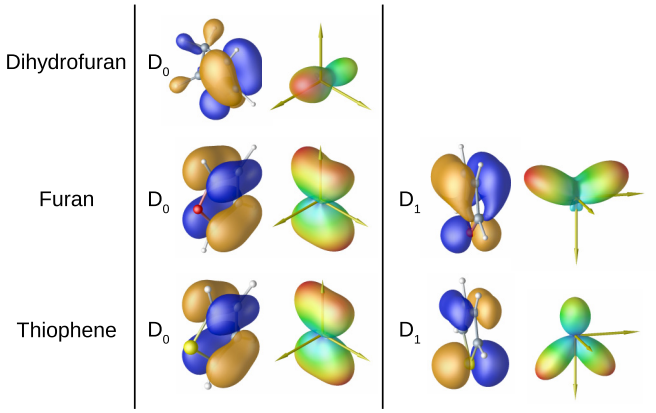

FIG. 3. Dyson orbitals (orange/blue plots) and the corresponding orientation dependence of the strong-field ionization yields for the non-negligible ionization channels of the molecules considered in this study.

We would now like to see the effect of the nodal planes in the ionized continuum electron wave packets. Consider first the continuum wave packets associated with the peaks in the orientation-dependent SFI yields. With the electric field of the laser polarized along the z-axis, we rotate each molecule such that they are oriented along the peaks of the orientation dependence of the SFI probabilities shown in Fig. 3, then we calculate the continuum wave packet using again the TD-RIS method. Note that the peak SFI probabilities for the D_0 and D_1 channels of both furan and thiophene are positioned at different angles, so we need to run the simulations at two different angles, one for the peak of the D_0 channel and a second angle corresponding to the peak of the D_1 channel.

Two-dimensional cuts through the computed three-dimensional continuum wave packets are plotted in Fig. 4. For these cuts, the electric field of the laser is aligned along the z axis, and the cuts are taken for a plane along $x = 0$ at the time $t = 0.375\tau_0$, where $\tau_0 = 2\pi/\omega_0$ is the period of the carrier oscillations of the laser. In these cuts, the center-of-mass of the molecules are positioned at the origin of coordinate system. For the cases where the peak of the orientation-dependent SFI yields lie away for the nodal planes (i.e., 2,3-dihydrofuran and the D_1 channels of furan and thiophene), the continuum wave packets exhibit a Gaussian-like distribution perpendicular to the electric field direction. For the D_0 channels of furan and thiophene, part of the nodal structure of the Dyson orbital is seen to persist into the continuum.

The corresponding transverse momentum distributions $\mathcal{D}(p_x, p_y)$ are shown in Fig. 5. To generate these transverse momentum distributions, we first take a cut of the continuum wave packet in a plane perpendicular to the electric field direction (z axis), $\Psi_{\rm cut}(x, y) = \Psi(x, y, z_0)$, where z_0 sets the position of the chosen plane along the z axis. In the following analysis, we use $z_0 = 15$ a.u., which lies comfortably away from the exponential tails of the Dyson orbitals but still close to the spatial point of birth of the continuum wave packet. Although there are quantitative difference when z_0 is varied, we checked that the conclusions of our analysis are independent of the particular choice of z_0 as long as it does not overlap with the tails of the initial bound orbital.

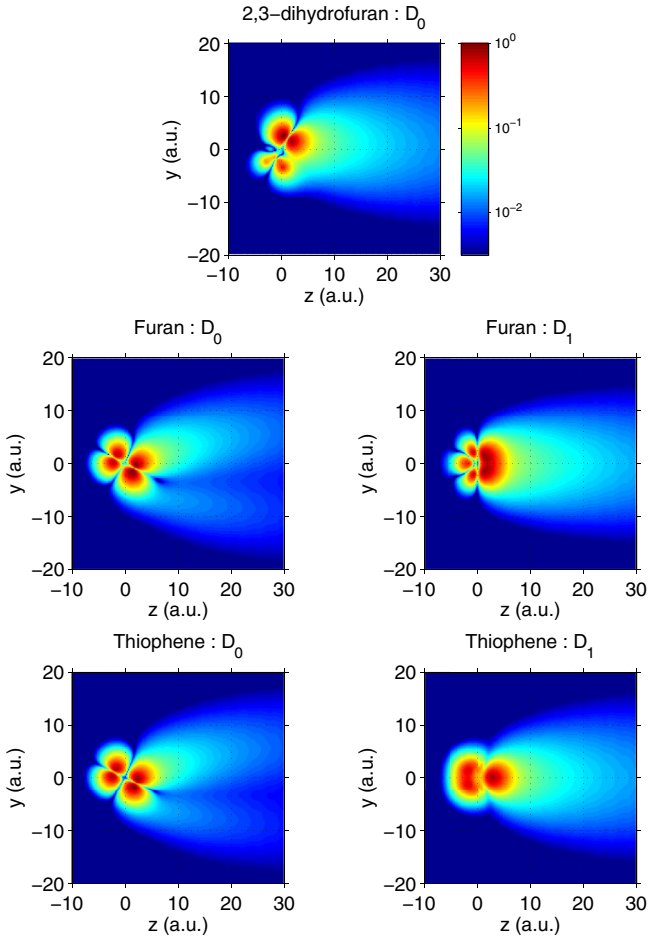

FIG. 4. Cut along the continuum wave function at the time $t = 0.375\ \tau_0$, where $\tau_0 = 2\pi/\omega_0$ is the period of the carrier oscillations of the laser. In these simulations, the electric field of the laser points toward the $-z$ direction, which pulls the negatively charged continuum electron toward the $+z$ direction.

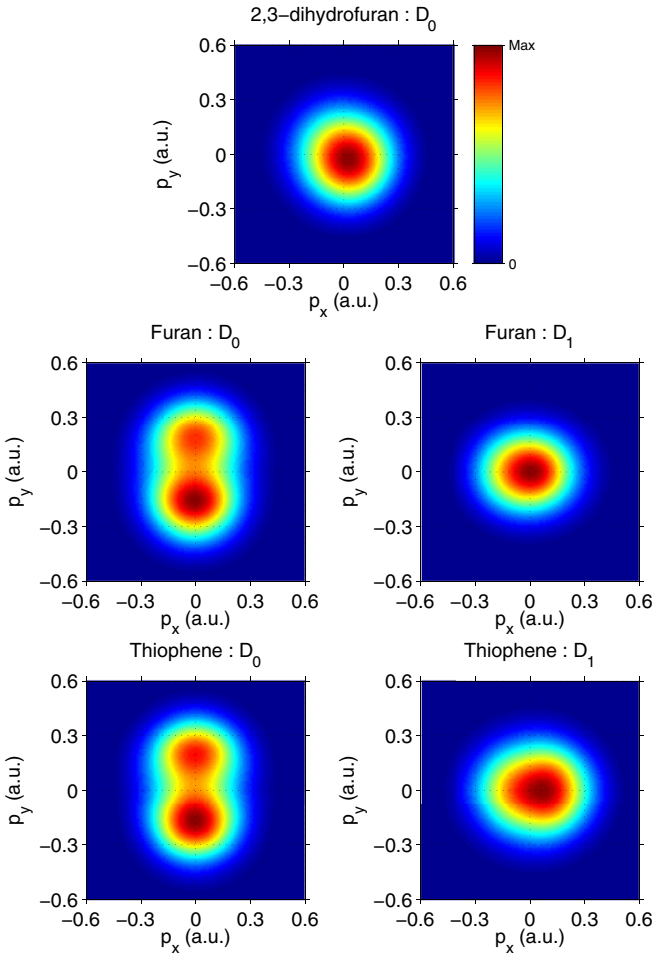

FIG. 5. Perpendicular momentum-space cuts of the continuum electron wave functions taken at the peak of the field ($t = \tau_0/4$), and $z = 15$ a.u. ($|\psi(p_x, p_y, z = 15\ \text{a.u.})|^2$), where z is the direction of the electric field vector of the ionizing laser. The cuts are qualitatively similar when taken at other times and at other z positions.

Figure 5 plots the corresponding transverse momentum distributions computed by taking the Fourier transform of the wave packet slice $\mathcal{D}(p_x, p_y) = |\mathcal{T}_F(\Psi_{\text{cut}})|^2$. From these plots, it is seen that $\mathcal{D}(p_x, p_y)$ is widest for the D_0 channels of furan and thiophene, the same two channels that had nodes in the continuum wave packets. Since the spatial and momentum representations of the wave function are related by the Fourier transform, the increased width seen in the momentum distributions are a direct consequence of the nodal structure in the continuum. Such an increase in the momentum width when ionizing along nodal directions has been noted in the literature [18–20]. The important feature of our study is that these effects of the nodal planes occur for the particular orientations where SFI is most probable.

The momentum distributions of the continuum wave packet plotted in Fig. 5 explain the differences seen in the ellipticity measurements. Furan and thiophene both exhibit ionization channels with wide momentum spreads (the D_0 channels). For these species, the large momentum spreads means that the recollision wave packet will be wider as compared to the 2,3-dihydrofuran case, and hence larger ellipticity is need to deflect the recollision wave packet and suppress the HHG emission. Although the above analysis considered only orientations that correspond to the peak ionization rates, it is clear from Fig. 3 that when averaging over all the orientations, the D_0 channels of furan and thiophene will show strong effects of the nodes in the continuum wave packet for the majority of orientations since the averaging will now encompass orientations that lie even close to, and directly along, nodal planes. Our interpretation is then robust to orientational averaging.

In summary, the ellipticity dependence of HHG provides information about the liberated continuum electron wave packet as well as the orientation dependence of SFI, even in the case of randomly oriented molecules. When the most probable orientation for SFI is near a nodal plane (furan and thiophene), the node of the ionizing orbital persists into the continuum wave packet thereby increasing the lateral momentum distribution, which leads to the observed differences in the ellipticity dependence of HHG for the studied molecular species. These theoretical and experimental findings draw into question the standard expectation that suppression of SFI should occur for orientations that lie along or near nodal planes of the ionizing orbitals.

[1] L. Keldysh, J. Exp. Theor. Phys. **20**, 1307 (1965).
[2] R. Freeman and P. Bucksbaum, J. Phys. B: At. Mol. Opt. Phys. **24**, 325 (1991).
[3] B. Sheehy and L. DiMauro, Annu. Rev. Phys. Chem. **47**, 463 (1996).
[4] V. Popov, Phy. Usp. **47**, 855 (2004).
[5] P. B. Corkum, Phys. Rev. Lett. **71**, 1994 (1993).
[6] M. Lewenstein, P. Balcou, M. Y. Ivanov, A. L'Huillier, and P. B. Corkum, Phys. Rev. A **49**, 2117 (1994).
[7] F. Krausz and M. Ivanov, Rev. Mod. Phys. **81**, 163 (2009).
[8] J. Itatani, J. Levesque, D. Zeidler, H. Niikura, H. Pepin, J. Kieffer, P. Corkum, and D. Villeneuve, Nature (London) **432**, 867 (2004).
[9] S. Haessler, J. Caillat, W. Boutu, C. Giovanetti-Teixeira, T. Ruchon, T. Auguste, Z. Diveki, P. Breger, A. Maquet, B. Carre, R. Taieb, and P. Salieres, Nat. Phys. **6**, 200 (2010).
[10] C. Vozzi, M. Negro, F. Calegari, G. Sansone, M. Nisoli, S. D. Silvestri, and S. Stagira, Nat. Phys. **7**, 822 (2011).
[11] H. Wörner, J. Bertrand, D. Kartashov, P. Corkum, and D. Villeneuve, Nature (London) **466**, 604 (2010).
[12] H. Wörner, J. Bertrand, B. Fabre, J. Higuet, H. Ruf, A. Dubrouil, S. Patchkovskii, M. Spanner, Y. Mairesse, V. Blanchet, E. Mével, E. Constant, P. Corkum, and D. Villeneuve, Science **334**, 208 (2011).
[13] M. C. H. Wong, A.-T. Le, A. F. Alharbi, A. E. Boguslavskiy, R. R. Lucchese, J.-P. Brichta, C. D. Lin, and V. R. Bhardwaj, Phys. Rev. Lett. **110**, 033006 (2013).
[14] R. Cireasa, A. E. Boguslavskiy, B. Pons, M. C. H. Wong, D. Descamps, S. Petit, H. Ruf, N. Thire, A. Ferré, J. Suarez, J. Higuet, B. E. Schmidt, A. F. Alharbi, F. Ferré, V. Blanchet, B. Fabre, S. Patchkovskii, O. Smirnova, Y. Mairesse, and V. R. Bhardwaj, Nat. Phys. **11**, 654 (2015).
[15] J. Muth-Böhm, A. Becker, and F. H. M. Faisal, Phys. Rev. Lett. **85**, 2280 (2000).
[16] O. Smirnova, Y. Mairesse, S. Patchkovskii, N. Dudovich, D. Villeneuve, P. Corkum, and M. Y. Ivanov, Nature (London) **460**, 972 (2009).
[17] M. Meckel, A. Staudte, S. Patchkovskii, D. Villeneuve, P. Corkum, R. Dörner, and M. Spanner, Nat. Phys. **10**, 594 (2014).
[18] T. Brabec, M. Côté, P. Boulanger, and L. Ramunno, Phys. Rev. Lett. **95**, 073001 (2005).
[19] L. Holmegaard, J. Hansen, L. Kalhøj, S. Kragh, H. Stapelfeldt, F. Filsinger, J. Küpper, G. Meijer, D. Dimitrovski, M. Abu-samha, C. Martiny, and L. Madsen, Nat. Phys. **6**, 428 (2010).
[20] I. Petersen, J. Henkel, and M. Lein, Phys. Rev. Lett. **114**, 103004 (2015).
[21] D. Dimitrovski, J. Maurer, H. Stapelfeldt, and L. B. Madsen, J. Phys. B: At. Mol. Opt. Phys. **48**, 245601 (2015).
[22] D. Pavičić, K. F. Lee, D. M. Rayner, P. B. Corkum, and D. M. Villeneuve, Phys. Rev. Lett. **98**, 243001 (2007).
[23] I. Thomann, R. Lock, V. Sharma, E. Gagnon, S. Pratt, H. Kapteyn, M. Murnane, and W. Li, J. Phys. Chem. A **112**, 9382 (2008).
[24] M. C. H. Wong, J.-P. Brichta, and V. R. Bhardwaj, Phys. Rev. A **81**, 061402 (2010).
[25] J. Mikosch, A. E. Boguslavskiy, I. Wilkinson, M. Spanner, S. Patchkovskii, and A. Stolow, Phys. Rev. Lett. **110**, 023004 (2013).
[26] K. S. Budil, P. Salières, A. L'Huillier, T. Ditmire, and M. D. Perry, Phys. Rev. A **48**, R3437(R) (1993).
[27] P. Dietrich, N. H. Burnett, M. Ivanov, and P. B. Corkum, Phys. Rev. A **50**, R3585(R) (1994).
[28] A. Perelomov, V. Popov, and M. Terent'ev, J. Exp. Theor. Phys. **24**, 207 (1967).
[29] N. B. Delone and V. P. Krainov, J. Opt. Soc. Am. B **8**, 1207 (1991).
[30] L. Arissian, C. Smeenk, F. Turner, C. Trallero, A. V. Sokolov, D. M. Villeneuve, A. Staudte, and P. B. Corkum, Phys. Rev. Lett. **105**, 133002 (2010).
[31] M. Spanner and S. Patchkovskii, Phys. Rev. A **80**, 063411 (2009).
[32] M. Spanner and S. Patchkovskii, Chem. Phys. **414**, 10 (2013).
[33] N. Thiré, S. Beaulieu, V. Cardin, A. Laramée, V. Wanie, B. E. Schmidt, and F. Légaré, Appl. Phys. Lett. **106**, 091110 (2015).
[34] V. V. Strelkov, M. A. Khokhlova, A. A. Gonoskov, I. A. Gonoskov, and M. Y. Ryabikin, Phys. Rev. A **86**, 013404 (2012).
[35] A. F. Alharbi, A. E. Boguslavskiy, N. Thiré, B. E. Schmidt, F. Légaré, T. Brabec, M. Spanner, and V. R. Bhardwaj, Phys. Rev. A **92**, 041801(R) (2015).
[36] D. Dimitrovski, J. Maurer, H. Stapelfeldt, and L. B. Madsen, Mol. Phys. **80**, 1431 (1993).